

# Multi-Physics Modeling of Light-Limited Microalgae Growth in Raceway Ponds

Andreas Nikolaou<sup>\*,\*\*</sup> Peter Booth<sup>\*</sup> Fraser Gordon<sup>\*</sup>  
Junfeng Yang<sup>\*</sup> Omar Matar<sup>\*</sup> Benoît Chachuat<sup>\*,\*\*</sup>

<sup>\*</sup> *Department of Chemical Engineering, Imperial College London,  
South Kensington Campus, London SW7 2AZ, UK.*

<sup>\*\*</sup> *Centre for Process Systems Engineering, Imperial College London,  
South Kensington Campus, London SW7 2AZ, UK.*

**Abstract:** This paper presents a multi-physics modeling methodology for the quantitative prediction of microalgae productivity in raceway ponds by combining a semi-mechanistic model of microalgae growth describing photoregulation, photoinhibition and photoacclimation, with models of imperfect mixing based on Lagrangian particle tracking and heterogeneous light distribution. The photosynthetic processes of photoproduction, photoregulation and photoinhibition are represented by a model of chlorophyll fluorescence developed by Nikolaou et al. (2015), which is extended to encompass photoacclimation. The flow is simulated with the commercial CFD package ANSYS, whereas light attenuation is described by the Beer-Lambert law as a first approximation. Full-scale simulation results are presented on extended time horizons. Comparisons are made in terms of areal productivities under both imperfect and idealized (CSTR) mixing conditions, and for various extraction rates and water depths.

**Keywords:** microalgae; raceway pond; photoinhibition; photoacclimation; CFD; imperfect mixing; light attenuation

## 1. INTRODUCTION

Phototrophic microorganisms—both microalgae and cyanobacteria—show a great potential for industrial applications, including food, pharmaceuticals and cosmetics, chemicals, and even biofuels. In comparison to conventional oil crops, they are independent from arable land and fresh water and can accumulate an array of useful by-products (Milledge, 2011). Moreover, lab- and pilot-scale experiments have shown that many microalgae species can achieve primary productivities orders of magnitude larger than terrestrial oil crops. The main commercial applications of microalgae so far have been concerned with high-value products, including carotenoids and omega-3 and omega-6 polyunsaturated fatty acids (Leu and Boussiba, 2014). In contrast, the commercial viability of microalgae as biofuel feedstock is still uncertain and calls for the development of large-scale outdoor raceway ponds to reduce production costs (Wijffels and Barbosa, 2010). Estimating the productivity of such systems based on a crude extrapolation from lab-scale experiments may be misleading due to drastically different conditions regarding access to light and nutrient, alongside imperfect mixing and temperature variations. In this context, mathematical modeling is a great help to understand, and in turn remedy, the gap between lab-scale observations and the industrial-scale reality (Béchet et al., 2013; Bernard et al., 2016). Not only are these models useful for analyzing and optimizing actual production systems, but they could also drive the choice

of a particular microalgae species that is best suited to the local environment or even to a particular season.

The modeling of high-density microalgae culture systems proves more challenging than that of bacterial or yeast culture systems. Part of this added complexity stems from the wide range of mechanisms that microalgae use to respond and adapt to light and other local environment factors, including photoregulation and photoacclimation whose dynamics range from seconds to days. Another challenge is tied to the fact that access to light inside the culture medium is highly heterogeneous due to light absorption, scattering and shadowing effects. Depending upon the mixing conditions, microalgae cells may be exposed to a range of different light irradiance levels over time scales of seconds or minutes—in addition to the diurnal light cycle.

The coupling of photosynthesis kinetics, hydrodynamics and light attenuation was first investigated some 40 years ago (Sheth et al., 1977), and many detailed models have been proposed since then for photobioreactors, using either an Eulerian or a Lagrangian description; see, e.g., Pruvost et al. (2008); Marshall and Sala (2011); Olivieri et al. (2015). Coupled models of outdoor raceway ponds were also developed during the early 1990s in the scope of the Aquatic Species Program (Sukenik et al., 1991). Recently, Hartmann et al. (2014) proposed an approach for modeling algae growth in raceway ponds using Lagrangian particle tracking, which allows reconstruction of the received light pattern, in combination with Han's model of photoproduction and photoinhibition (Han, 2002).

<sup>\*</sup> This work was financial supported by Marie Curie Career Integration Grant PCIG09-GA-2011-293953 (DOP-ECOS).

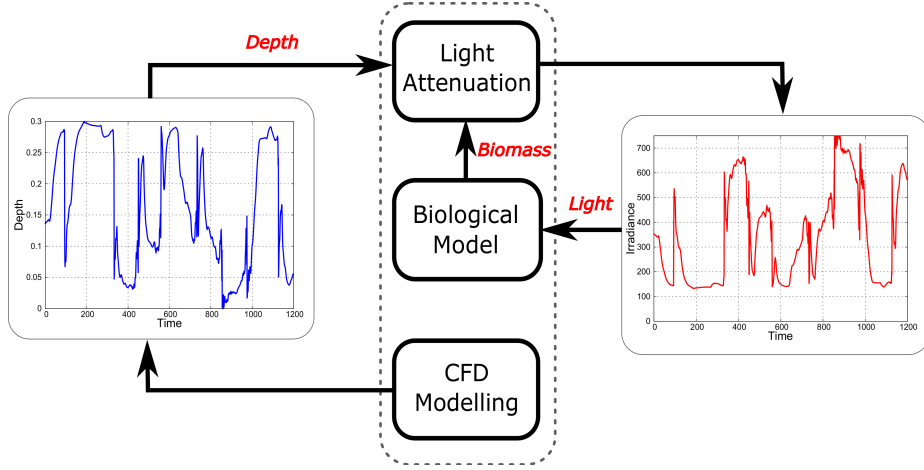


Fig. 1. Coupling methodology of photosynthesis kinetics, hydrodynamics and light attenuation in the raceway pond.

This paper proposes an improved multi-physics model of microalgae raceway ponds by combining a semi-mechanistic model of microalgae growth describing photoregulation, photoinhibition and photoacclimation, with models of imperfect mixing based on Lagrangian particle tracking and heterogeneous light distribution. This model and the coupling methodology are presented in Sect. 2. The algal growth kinetics are based on the chlorophyll fluorescence model by Nikolaou et al. (2015) and feature a novel extension to account for photoacclimation. Moreover, the flow is simulated with the commercial CFD package ANSYS, whereas light attenuation is described by the Beer-Lambert law as a first approximation. The numerical implementation is discussed in Sect. 3, before presenting full-scale simulation results on extended time horizons. Comparisons are made in terms of areal productivities under both imperfect and idealized (CSTR) mixing conditions, and for various extraction rates and water depths. Finally, Sect. 4 concludes the paper.

## 2. MULTI-PHYSICS MODELING METHODOLOGY

The overall modeling methodology is depicted in Fig. 1. A commercial CFD package (ANSYS) is used to simulate the velocity field inside the raceway pond, and subsequently obtain a large number of particle trajectories for which light histories are generated via the light attenuation model. These light histories are then passed to the biological model in order to predict primary production along the individual trajectories. The overall productivity of the raceway pond is obtained by averaging over all the trajectories. The following two simplifications are adopted in order to make the coupling sequential and tractable: (i) the velocity field is unaffected by the microalgae cells in suspension; and (ii) the concentration and composition of microalgae cells inside the pond is uniform in terms of their light attenuation effect. Moreover, we consider nutrient-replete conditions and assume no limitation by  $\text{CO}_2$  or temperature for the scope of this paper.

### 2.1 Microalgae Growth Kinetics

The model by Nikolaou et al. (2015) predicts fluorescence fluxes by taking into account the state of the photosystem II (RCII) and the activity of photoregulation (NPQ).

These fluxes can then be related to the growth rate as (Bernardi et al., 2015, 2016)

$$\mu = \left( I \sigma \nu \frac{A \eta_P}{1 + \eta_D + \eta_{QE} \alpha + A \eta_P + C \eta_I} - R \right) \theta \quad (1)$$

$$\dot{A} = -I \sigma_{PS2} A + \frac{B}{\tau} \quad (2)$$

$$\dot{B} = I \sigma_{PS2} A - \frac{B}{\tau} + k_r C - k_d \sigma_{PS2} I B \quad (3)$$

$$\dot{C} = -k_r C + k_d \sigma_{PS2} I B \quad (4)$$

$$\Phi_f^A = \frac{1}{1 + \eta_P + \eta_D + \eta_{QE} \alpha} \quad (5)$$

$$\Phi_f^B = \frac{1}{1 + \eta_D + \eta_{QE} \alpha} \quad (6)$$

$$\Phi_f^C = \frac{1}{1 + \eta_I + \eta_D + \eta_{QE} \alpha} \quad (7)$$

$$\alpha = \xi \left( \alpha - \frac{I^n}{I_{QE}^n + I^n} \right) \quad (8)$$

$$\sigma_{PS2} = \frac{\sigma \eta_P}{N(1 + \eta_D + \eta_{QE} \alpha + \eta_P)} \quad (9)$$

The growth rate  $\mu$  [ $\text{s}^{-1}$ ] in Eq. (1) is proportional to the chlorophyll-to-carbon quota,  $\theta$  [ $\text{g}_{\text{chl}} \text{g}_C^{-1}$ ]. It is also a function of the incoming light intensity,  $I$  [ $\mu\text{E m}^{-2} \text{s}^{-1}$ ], the total cross-section,  $\sigma$  [ $\text{m}^2 \text{g}_{\text{chl}}^{-1}$ ] and the respiration rate parameter,  $R$  [ $\text{g}_C \text{g}_{\text{chl}}^{-1} \text{s}^{-1}$ ], where  $\nu$  is a stoichiometric coefficient between electron flow and carbon fixation. Following the model by Han (2002), Eqs. (2)-(4) describe transitions of the reaction centers of photosystem II (RCII) between active,  $A$  [-], occupied,  $B$  [-] and damaged,  $C$  [-] states, as a function of  $I$ . Photoproduction is described by the transition  $A \rightleftharpoons B$ , which depends on the effective cross section,  $\sigma_{PS2}$  [ $\text{m}^2 \mu\text{E}^{-1}$ ] and turnover time,  $\tau$  [s] of RCII. Photoinhibition is described by the transition  $B \rightleftharpoons C$ , which depends on damage,  $k_d$  [-] and repair,  $k_r$  [ $\text{s}^{-1}$ ] constants. The fluorescence quantum yields for each RCII state,  $\Phi_f^A$  [-],  $\Phi_f^B$  [-] and  $\Phi_f^C$  [-] given by Eqs. (5)-(7), depend on the dimensionless parameters  $\eta_P$ ,  $\eta_D$ ,  $\eta_I$  and  $\eta_{QE}$ . The NPQ activity,  $\alpha$  [-] in Eq. (8) tracks a sigmoidal set-point function of  $I$ , with parameters  $I_{QE}$  [ $\mu\text{E m}^{-2} \text{s}^{-1}$ ] and  $n$  [-]. Finally, Eq. (9) relates  $\sigma_{PS2}$  with the number of RCII,  $N$  [ $\mu\text{E g}_{\text{chl}}^{-1}$ ],  $\sigma$  and  $\alpha$ .

Table 1. Estimated acclimation and respiration parameter values.

Parameter	Calibrated value	Units
$\delta$	$1.38 \times 10^{-1}$	—
$\theta_0$	$3.60 \times 10^0$	$g_{chl} g_C^{-1}$
$\kappa$	$-1.89 \times 10^{-1}$	—
$N_0$	$1.71 \times 10^0$	$\mu E g_{chl}^{-1}$
$\lambda$	$1.22 \times 10^{-1}$	—
$I_{qE,0}$	$8.13 \times 10^2$	$\mu E m^{-2} s^{-1}$
$\epsilon$	$4.48 \times 10^{-1}$	—
$R$	$1.78 \times 10^{-5}$	$g_C g_{chl}^{-1} s^{-1}$

Bernard (2011) argues that photoacclimation dynamics can be described in terms of variations of the so-called acclimation irradiance,  $I_g [\mu E m^{-2} s^{-1}]$  as

$$\dot{I}_g = \delta(I - I_g)\mu, \quad (10)$$

where  $\delta [-]$  is a constant proportionality coefficient representing the rate of photoacclimation. The link between Eq. (10) and the kinetic model (1)-(9) is established through empirical acclimation rules that relate the variables  $\theta$ ,  $N$  and  $I_{qE}$  to the acclimation state,  $I_g$ :

- The variation in the pigment content of the cells due to photoacclimation is described by power laws relating the chlorophyll-to-carbon quota,  $\theta$  and the number of RCII,  $N$  to the acclimation state,  $I_g$  as (Fisher et al., 1996; MacIntyre et al., 2002; Nikolaou et al., 2016)

$$\theta = \theta_0 (I_g)^\kappa, \quad (11)$$

$$N = N_0 (I_g)^\lambda, \quad (12)$$

with acclimation parameters  $\theta_0$ ,  $N_0$ ,  $\kappa$  and  $\lambda$ .

- The variation in the carotenoid-to-chlorophyll ratio of the cells due to photoacclimation impacts the dissipation of excess energy via NPQ regulation and is captured by a simple linear law relating  $I_{qE}$  with  $I_g$  as (Simionato et al., 2011)

$$I_{qE} = I_{qE,0} + \epsilon I_g, \quad (13)$$

with corresponding acclimation parameters  $I_0$  and  $\epsilon$ .

The rationale behind the choice of the acclimation rules (11)–(13) is that they provide a minimal model complexity for accurate prediction of a set of experimental data for the microalga *Nannochloropsis gaditana*, while still providing statistically confident estimates.

The overall growth model (1)–(13) accounts for photoproduction, photoregulation, photoinhibition and photoacclimation all together, and its dynamics span many time-scales ranging from milliseconds to days. Due to space restriction we only report the estimated values of the extra acclimation and respiration parameter in Table 1 and refer the reader to Nikolaou (2015) for further details; the remaining parameters  $\eta_D$ ,  $\eta_P$ ,  $\eta_I$ ,  $\eta_{qE}$ ,  $\tau$ ,  $k_d$ ,  $k_r$ ,  $\xi$ ,  $n$ ,  $\sigma$  are set to the values given in Nikolaou et al. (2015).

## 2.2 Hydrodynamics

Modeling of the flow conditions inside the raceway pond is carried out in the commercial package ANSYS 15 (<http://www.ansys.com/>), based on an existing raceway pond at INRA Narbonne, France (Hreiz et al., 2014). This raceway is equipped with a paddlewheel (Fig. 2) and the water depth is set to  $H = 0.3$  m (liquid volume of  $15.8 \text{ m}^3$ ) for the

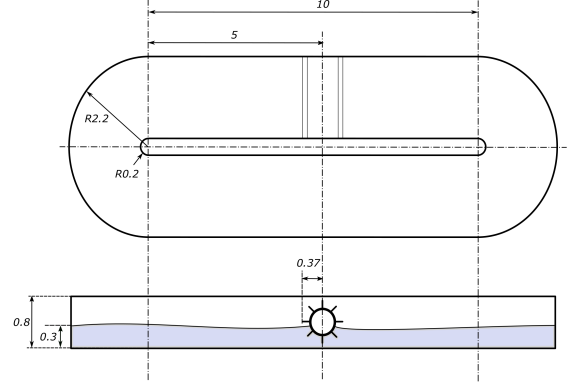


Fig. 2. Geometrical characteristics of the raceway pond.

simulation. A tetrahedral structured mesh with 209,960 nodes and 183,615 elements is used for the 3-d simulation, which allows for a vertical discretization of the liquid phase into 20 layers. This mesh is further divided into two parts: (i) a finely discretized, sliding mesh of cylindrical shape surrounding the paddle-wheel and rotating around its axis at an angular velocity of 10 rpm; and (ii) a stationary mesh including the remaining computational domain. The code FLUENT is used to solve the Reynolds averaged Navier-Stokes equations in transient mode, with a time step of 0.01 s. The implicit compressive scheme of the volume of fluid (VOF) model is used to track the free surface of water and air, which has a surface tension coefficient of  $71.99 \text{ mN m}^{-1}$  at  $25^\circ\text{C}$ . The realizable  $\kappa$ - $\epsilon$  model with default parameter values is used to represent turbulence, the convective terms are discretized using the QUICK scheme, and the diffusion terms are central-differenced.

The simulation itself is divided into two parts.

- (1) During the first 1,200 seconds of the simulation, the raceway pond is initialized from a resting state to a stabilized flow. The velocity field at 0.2 m above the raceway floor at the end of this period is illustrated in Fig. 3. The flow is turbulent near the paddlewheel and mostly laminar elsewhere. The inner bends of the pond are seen to cause a flow acceleration, whereas dead zones develop near the outer bends and at the inner side of the channel opposite the paddle-wheel.

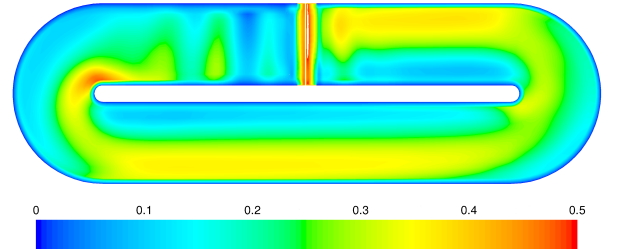


Fig. 3. Mean velocity magnitude at 0.2 m above the raceway floor.

- (2) During the subsequent 1,200 seconds of the simulation, 2000 particles are injected in the raceway pond and their positions are recorded every second of simulation (Lagrangian particle tracking) using a dedicated C-code. The particles have a diameter of  $5 \mu\text{m}$  to resemble the size of *N. gaditana* and are

initialized with the velocity of the flow at their points of injection. Two selected trajectories are represented in Fig. 4 during 600 seconds, where the depth of the particles is seen to fluctuate considerably. The most important factor affecting the vertical position is the paddle-wheel rotation, which can push a particle up or down, depending on its position as it nears the paddles. The bends of the pond are also found to have an effect on the vertical position of the particles due to local velocity gradients.

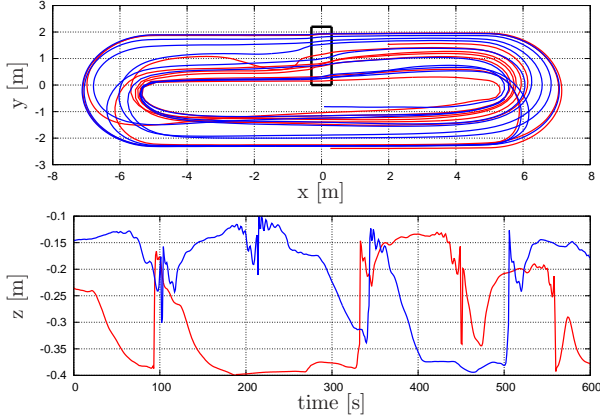


Fig. 4. horizontal position (upper plot) and depth histories (lower plot) for two selected trajectories.

### 2.3 Light Attenuation

Since the commercial viability of microalgae production systems calls for denser cultures, accounting for light attenuation is indeed paramount. As a first approximation, the light attenuation caused by both absorption by pigments and scattering by biomass particles may be predicted using Beer-Lambert's law as (Bernard, 2011)

$$I_z = I_0 \exp(-[E_s(X + X_d) + E_a X \theta]z), \quad (14)$$

where  $I_0$  and  $I_z$  [ $\mu\text{E m}^{-2} \text{s}^{-1}$ ] stand for the light intensities at the surface and at a depth  $z$  [m] inside the culture, respectively. The light attenuation in Eq. (14) increases with the active and dead biomass concentrations,  $X$  and  $X_d$  [ $\text{g}_C \text{L}^{-1}$ ], and with the chlorophyll concentration,  $X\theta$  [ $\text{g}_{chl} \text{L}^{-1}$ ]. The proportionality coefficient  $E_a$  [ $\text{m}^2 \text{g}_{chl}^{-1}$ ] accounts for light absorption by pigment molecules, whereas  $E_s$  [ $\text{m}^2 \text{g}_C^{-1}$ ] accounts for light scattering by biomass particles. These coefficients are set to  $E_a = 0.20 \times 10^2 \text{ m}^2 \text{g}_C^{-1}$  and  $E_s = 0.10 \times 10^2 \text{ m}^2 \text{g}_{chl}^{-1}$  thereafter, in agreement with the light attenuation ranges given by Sevilla and Grima (1997). Moreover, the incoming light intensity is set to follow a diurnal pattern given by the sinusoidal function

$$I_0(t) = I_{\max} \frac{[1 - \cos(\frac{2\pi t}{86400})]^3}{8}, \quad (15)$$

with the mid-day irradiance  $I_{\max} = 1200 \mu\text{E m}^{-2} \text{s}^{-1}$  representative of Southern Europe during the summer.

### 2.4 Multi-Physics Coupling

*Imperfect Mixing Case* In order to simulate the raceway pond at scale, the idea is to integrate the microalgae growth model (1)-(13) through time along each Lagrangian

trajectory  $j = 1, \dots, N_{\text{traj}}$ . Subsequently, the state variables in the growth model are indexed with  $j$  in reference to the  $j$ th trajectory, such as  $\mu_j(t)$ ,  $\theta_j(t)$ ,  $I_{g,j}(t)$ , and the depth and local irradiance histories are denoted by  $z_j(t)$  and  $I_j(t)$  likewise.

Following mass conservation principles, the local variations in active and dead biomass concentrations,  $X_j(t)$  and  $X_{d,j}(t)$  are given by

$$\dot{X}_j(t) = (\mu_j(t) - D)X_j(t), \quad (16)$$

$$\dot{X}_{d,j}(t) = R X_j(t) - D X_{d,j}(t), \quad (17)$$

where  $D$  [ $\text{s}^{-1}$ ] is the dilution rate. Then, per the assumption that the concentration and composition of microalgae cells inside the pond are uniform in terms of their light attenuation effect, the coupling between the growth kinetics and the light attenuation along each trajectories follows from Eq. (14) in the form

$I_j(t) = I_0(t) \exp(-[E_s(\bar{X}(t) + \bar{X}_d(t)) + E_a \bar{X}(t) \bar{\theta}(t)]z_j(t))$ , where the average active and dead biomass concentrations,  $\bar{X}(t)$  and  $\bar{X}_d(t)$ , and the average chlorophyll quota,  $\bar{\theta}$ , are calculated over all the Lagrangian trajectories as

$$\bar{X}(t) = \frac{1}{N_{\text{traj}}} \sum_{j=1}^{N_{\text{traj}}} X_j, \quad \bar{X}_d(t) = \frac{1}{N_{\text{traj}}} \sum_{j=1}^{N_{\text{traj}}} X_{d,j},$$

$$\bar{\theta}(t) = \frac{1}{N_{\text{traj}}} \sum_{j=1}^{N_{\text{traj}}} \theta_j(t).$$

The corresponding areal (net) primary productivity,  $P$  [ $\text{g}_C \text{L}^{-1} \text{s}^{-1}$ ] for the pond is given by

$$P(t) = \frac{1}{N_{\text{traj}}} \sum_{j=1}^{N_{\text{traj}}} \mu_j(t) X_j(t), \quad (18)$$

and possibly averaged over a 24-hour period to obtain the daily-average (net) primary productivity.

*Perfect Mixing (CSTR) Case* In addition to the assumption of a uniform biomass concentration and composition with regards to light attenuation, this idealized case assumes that the microalgae cells are all identical in terms of their photosynthetic states. Unlike the imperfect mixing case above where the cells follow separate depth and light histories along the Lagrangian trajectories, perfect mixing considers for all the cells to have an equi-probable exposure to light across the water column.

The average photosynthetic state of the cells is described by integro-differential equations of the form

$$\dot{\bar{I}}_g(t) = \frac{1}{H} \int_0^H \delta[I_z(t) - \bar{I}_g(t)] \bar{\mu}(t) dz,$$

with  $I_z$  as given in Eq. (14), and the like for the other averaged quantities  $\bar{\mu}$ ,  $\bar{A}$ ,  $\bar{B}$ , ... in Eqs. (1)-(13). Then, the average active and dead biomass concentrations,  $\bar{X}(t)$  and  $\bar{X}_d(t)$  are obtained from

$$\dot{\bar{X}}(t) = (\bar{\mu}(t) - D) \bar{X}(t),$$

$$\dot{\bar{X}}_d(t) = R \bar{X}(t) - D \bar{X}_d(t),$$

and the areal (net) primary productivity is given by

$$P(t) = \bar{\mu}(t) \bar{X}(t).$$



### 3. RESULTS AND DISCUSSIONS

The multi-physics model based on Lagrangian particle tracking and heterogeneous light distribution is comprised of a large set of differential equations, for which a numerical solution can be obtained with state-of-the-art numerical integrators such as CVODE-SUNDIALS (<https://computation.llnl.gov/casc/sundials/>). In order to run simulations on extended time horizons of several weeks, the Lagrangian trajectories computed with ANSYS (timespan of 1,200 seconds) are applied repeatedly based on a randomization over all the available trajectories at the paddle-wheel. Using a variable-order BDF method with a diagonal approximation of the Jacobian matrix and tight relative and absolute local error tolerances of, respectively,  $10^{-7}$  and  $10^{-10}$ , a one-day simulation of the raceway takes about 210 CPU-seconds with  $N_{\text{traj}} = 200$  Lagrangian trajectories and 570 CPU-seconds with  $N_{\text{traj}} = 500$  on a recent laptop computer.<sup>1</sup> Moreover, no appreciable differences are observed for results computed with 200 trajectories or more.

The results of a full-scale dynamic simulation of the raceway pond are shown in Fig. 5 for a constant dilution rate of  $D = 0.25 \text{ day}^{-1}$  and water depth of  $H = 0.30 \text{ m}$ , and with an initial (active) biomass concentration of  $100 \text{ mg}_C \text{ L}^{-1}$ . Both the active and dead biomass concentration profiles reach a cyclic steady-state regime—due to the diurnal light pattern imposed through Eq. (15)—within several weeks of simulated time; as light attenuation in the culture increases with the concentrations of active and dead biomass, the rate of increase in active biomass during daytime progressively slows down until the point that it is balanced by the rate of respiration. Moreover, the daily variations in active biomass are expectedly larger than those in dead biomass, given that biomass decay occurs steadily during the day, unlike biomass growth.

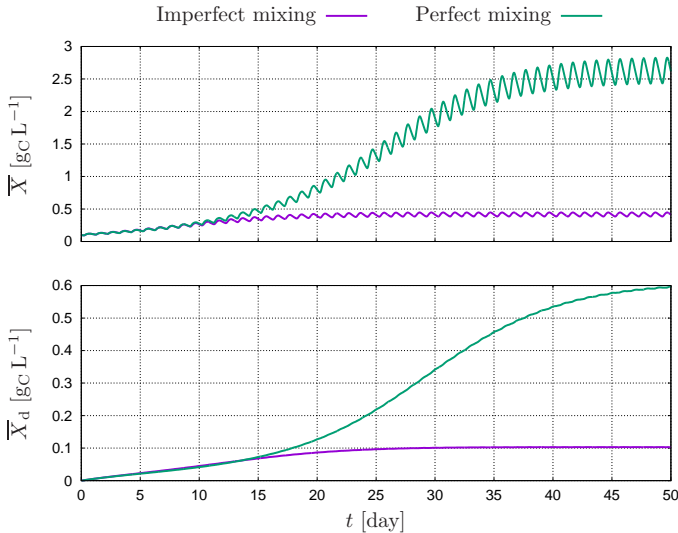


Fig. 5. Evolution of the active (top plot) and dead (bottom plot) biomass over 50 days for the multi-physics model under either imperfect or perfect mixing.

Under imperfect mixing conditions, the daily average concentration of active and dead biomass reach ca.

<sup>1</sup> Intel Core i7-3687U CPU @2.10GHz×4, running Ubuntu 14.04 LTS 64 bits and gcc version 4.8.4.

$410 \text{ mg}_C \text{ L}^{-1}$  and  $100 \text{ mg}_C \text{ L}^{-1}$ , respectively. These values are 6 to 7-fold lower than their counterparts in the idealized case of perfect mixing, respectively, ca.  $2630 \text{ mg}_C \text{ L}^{-1}$  and  $610 \text{ mg}_C \text{ L}^{-1}$ . These results thus provide a clear confirmation that a large part of the loss in microalgae productivity that is observed in going from lab to industrial scale is attributable to imperfect mixing.

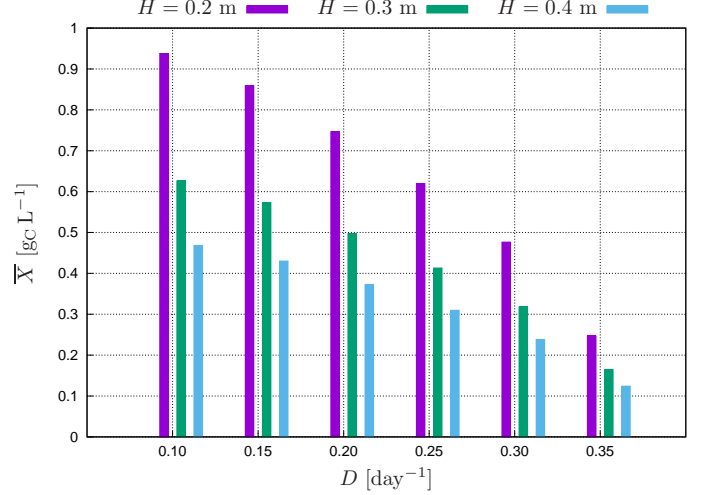


Fig. 6. Active biomass concentrations at cyclic steady-state (24-hour average) for operations at various dilution rates  $D$  and water depths  $H$ .

A comparison of the realizable active biomass concentrations for various dilution rate values  $D$  in the range  $0.1\text{--}0.4 \text{ day}^{-1}$  and water depths  $H$  between  $0.2\text{--}0.4 \text{ m}$  is shown in Fig. 6. Note that different water depths are simulated here via direct scaling of the trajectory depth histories from the CFD base case of  $H = 0.3 \text{ m}$ , instead of recomputing the Lagrangian trajectories anew for  $H = 0.2 \text{ m}$  and  $0.4 \text{ m}$ . At a given dilution rate, the realizable biomass concentration decreases as the water depth increases due to the effect of light attenuation through the water column. Overall, these projections show that cultures of *N. gaditana* denser than  $1 \text{ g}_C \text{ L}^{-1}$  may hardly be grown in traditional raceways.

Quite remarkably, the realizable areal net productivities—computed from Eq. 18—turn out to be equal for all three water depths. These areal productivities are plotted in Fig. 7 for various dilution rates, under both imperfect and perfect mixing conditions. In either cases, the areal productivity passes through a maximum for a dilution rate between  $0.2\text{--}0.25 \text{ day}^{-1}$ . This maximum is ca.  $20 \text{ g}_C \text{ m}^{-2} \text{ day}^{-1}$  in the imperfect mixing case, which is again about 7-fold lower than the predicted value of  $135 \text{ g}_C \text{ m}^{-2} \text{ day}^{-1}$  under a perfect mixing scenario. Assuming (dry) biomass to have a carbon content of 50%, this gives an areal biomass productivity for the pond around  $0.04 \text{ kg m}^{-2} \text{ day}^{-1}$ , which is close to the projected productivity of  $0.035 \text{ kg m}^{-2} \text{ day}^{-1}$  by Chisti (2007).

To finish, we shall revisit the main modeling simplifications formulated in Sect. 2. The assumption that the velocity field is unaffected by the microalgae suspension turns out to be reasonable since the viscosity of the culture medium is about the same as water for microalgae suspensions with a volume fraction less than 1% (several grams per liter) (Zhang et al., 2013). Moreover, the assumption of

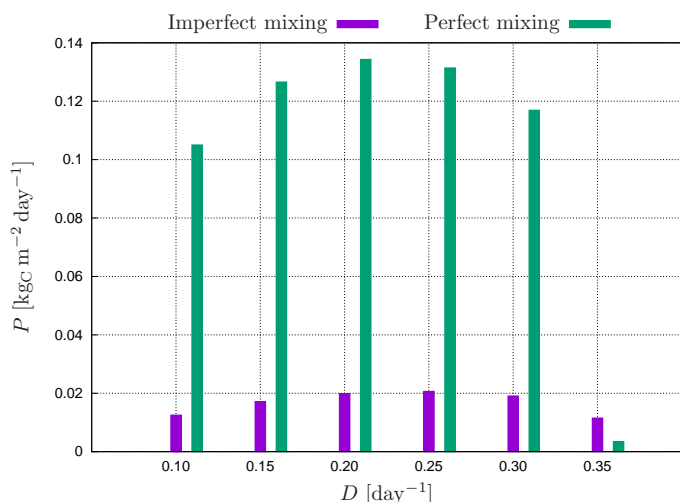


Fig. 7. Net primary production at cyclic steady-state (24-hour average) for the multi-physics model with imperfect mixing compared to the idealized perfect mixing case at various dilution rates  $D$ .

a uniform biomass concentration in the raceway is supported by experimental observations in Hreiz et al. (2014), although it may not hold for bigger raceways. Lastly, it is worth reemphasizing that the projected productivities are inherently optimistic as microalgae growth is both nutrient- and temperature-limited in practice.

#### 4. CONCLUSIONS AND FUTURE DIRECTIONS

The proposed modeling framework is the first of its kind to couple a detailed algal growth kinetic model describing photoregulation, photoinhibition and photoacclimation all together, with a CFD model of imperfect mixing based on Lagrangian particle tracking and heterogeneous light distribution. This allows for realistic extrapolation of lab-scale measurements based on fluorometry and respirometry to full-scale production in raceway ponds. Such extrapolation capability may find applications for the screening of microalgae strains or even to guide the development of mutants for improved productivities in targeted geographical regions. This generic simulation capability may also find applications in design and operations optimization of raceway ponds. As part of future work, it will be interesting to extend the present framework to encompass both nutrient- and temperature-limited growth for more realistic predictions.

#### REFERENCES

Béchet, Q., Shilton, A., and Guieysse, B. (2013). Modeling the effects of light and temperature on algae growth: State of the art and critical assessment for productivity prediction during outdoor cultivation. *Biotechnol. Adv.*, 31(8), 1648–1663.

Bernard, O. (2011). Hurdles and challenges for modelling and control of microalgae for CO<sub>2</sub> mitigation and biofuel production. *J. Process Control*, 21(10), 1378–1389.

Bernard, O., Mairet, F., and Chachuat, B. (2016). Modelling of microalgae culture systems with applications to control and optimization. *Adv. Biochem. Eng. Biotechnol.*, 153, 59–87.

Bernardi, A., Nikolaou, A., Meneghesso, A., Morosinotto, T., Chachuat, B., and Bezzo, F. (2015). A framework for dynamic modeling of PI curves in microalgae. *Comput. Aided Chem. Eng.*, 37, 2483–2488.

Bernardi, A., Nikolaou, A., Meneghesso, A., Morosinotto, T., Chachuat, B., and Bezzo, F. (2016). High-fidelity modelling methodology of light-limited photosynthetic production in microalgae. *PLoS ONE*, in press.

Chisti, Y. (2007). Biodiesel from microalgae. *Biotechnol. Adv.*, 25(3), 294–306.

Fisher, T., Minnaard, J., and Dubinsky, Z. (1996). Photoacclimation in the marine alga *Nannochloropsis* sp. (eustigmatophyte): A kinetic study. *J. Plankton Res.*, 18(10), 1797–1818.

Han, B.P. (2002). A mechanistic model of algal photoinhibition induced by photodamage to photosystem-II. *J. Theor. Biol.*, 214(4), 519–27.

Hartmann, P., Combe, C., Rabouille, S., Sciandra, A., and Bernard, O. (2014). Impact of hydrodynamics on single cell algal photosynthesis in raceways: characterization of the hydrodynamic system and light patterns. In *Proc. 19th IFAC World Congress*.

Hreiz, R., Sialve, B., Morchain, J., Escudié, R., Steyer, J.P., and Guiraud, P. (2014). Experimental and numerical investigation of hydrodynamics in raceway reactors used for algaculture. *Chem. Eng. J.*, 250, 230–239.

Leu, S. and Boussiba, S. (2014). Advances in the production of high-value products by microalgae. *Ind. Biotechnol.*, 10(3), 169–183.

MacIntyre, H.L., Kana, T.M., Anning, T., and Geider, R.J. (2002). Photoacclimation of photosynthesis irradiance response curves and photosynthetic pigments in microalgae and cyanobacteria. *J. Appl. Phycol.*, 38(1), 17–38.

Marshall, J.S. and Sala, K. (2011). A stochastic Lagrangian approach for simulating the effect of turbulent mixing on algae growth rate in a photobioreactor. *Chem. Eng. Sci.*, 66(3), 384–392.

Milledge, J.J. (2011). Commercial application of microalgae other than as biofuels: a brief review. *Rev. Environ. Sci. Biotechnol.*, 10(1), 31–41.

Nikolaou, A. (2015). *Multi-scale Modeling of Light-limited Growth in Microalgae Production Systems*. Ph.D. thesis, Dpt. Chemical Engineering, Imperial College London, UK.

Nikolaou, A., Bernardi, A., Meneghesso, A., Bezzo, F., Morosinotto, T., and Chachuat, B. (2015). A model of chlorophyll fluorescence in microalgae integrating photoproduction, photoinhibition and photoregulation. *J. Biotechnol.*, 194, 91–99.

Nikolaou, A., Hartmann, P., Sciandra, A., Chachuat, B., and Bernard, O. (2016). Dynamic coupling of photoacclimation and photoinhibition in a model of microalgae growth. *J. Theor. Biol.*, 390, 61–72.

Olivieri, G., Gargiulo, L., Lettieri, P., Mazzei, L., Salatino, P., and Marzocchella, A. (2015). Photobioreactors for microalgal cultures: A Lagrangian model coupling hydrodynamics and kinetics. *Biotechnol. Progr.*, 31(5), 1259–1272.

Pruvost, J., Cornet, J.F., and Legrand, J. (2008). Hydrodynamics influence on light conversion in photobioreactors: An energetically consistent analysis. *Chem. Eng. Sci.*, 63(8), 1648–1663.

Sevilla, J. and Grima, E.M. (1997). A model for light distribution and average solar irradiance inside outdoor tubular photobioreactors for the microalgal mass culture. *Biotechnol. Bioeng.*, 55(5), 701.

Sheth, M., Ramkrishna, D., and Fredrickson, A.G. (1977). Stochastic models of algal photosynthesis in turbulent channel flow. *AIChE J.*, 23(6), 794–804.

Simionato, D., Sforza, E., Corteggiani Carpinelli, E., Bertucco, A., Giacometti, G.M., and Morosinotto, T. (2011). Acclimation of *Nannochloropsis gaditana* to different illumination regimes: Effects on lipids accumulation. *Bioresour. Technol.*, 102(10), 6026–6032.

Sukenik, A., Levy, R.S., Levy, y., Falkowski, P.G., and Dubinsky, Z. (1991). Optimizing algal biomass production in an outdoor pond: a simulation model. *J. Appl. Phycol.*, 3, 191–201.

Wijffels, R.H. and Barbosa, M.J. (2010). An outlook on microalgal biofuels. *Science*, 329(5993), 796–799.

Zhang, X., Jiang, Z., Chen, L., Chou, A., Yan, H., Zuo, Y.Y., and Zhang, X. (2013). Influence of cell properties on rheological characterization of microalgae suspensions. *Bioresour. Technol.*, 139, 209–213.